Photoemission Spectroscopic Evidence for the Dirac Nodal Line in the Monoclinic Semimetal $SrAs_3$

Y. K. Song,[1,2,3,*] G. W. Wang,[4,*] S. C. Li,[5] W. L. Liu,[1,2,3] X. L. Lu,[1,6] Z. T. Liu,[1] Z. J. Li,[1] J. S. Wen,[5,7] Z. P. Yin,[4,†] Z. H. Liu,[1,‡] and D. W. Shen[1,2,§]

[1]*Center for Excellence in Superconducting Electronics, State Key Laboratory of Functional Materials for Informatics, Shanghai Institute of Microsystem and Information Technology, Chinese Academy of Sciences, Shanghai 200050, China*
[2]*Center of Materials Science and Optoelectronics Engineering, University of Chinese Academy of Sciences, Beijing 100049, China*
[3]*School of Physical Science and Technology, ShanghaiTech University, Shanghai 200031, China*
[4]*Department of Physics and Center for Advanced Quantum Studies, Beijing Normal University, Beijing 100875, China*
[5]*National Laboratory of Solid State Microstructures and Department of Physics, Nanjing University, Nanjing 210093, China*
[6]*University of Chinese Academy of Sciences, Beijing 100049, China*
[7]*Collaborative Innovation Center of Advanced Microstructures, Nanjing University, Nanjing 210093, China*

(Received 23 August 2019; revised manuscript received 2 January 2020; accepted 10 January 2020; published 7 February 2020)

Topological nodal-line semimetals with exotic quantum properties are characterized by symmetry-protected line-contact bulk band crossings in the momentum space. However, in most of identified topological nodal-line compounds, these topological nontrivial nodal lines are enclosed by complicated topological trivial states at the Fermi energy (E_F), which would perplex their identification and hinder further applications. Utilizing angle-resolved photoemission spectroscopy and first-principles calculations, we provide compelling evidence for the existence of Dirac nodal-line fermions in the monoclinic semimetal $SrAs_3$, which possesses a simple nodal loop in the vicinity of E_F without the distraction from complicated trivial Fermi surfaces. Our calculations revealed that two bands with opposite parities were inverted around Y near E_F, resulting in the single nodal loop at the Γ-Y-S plane with a negligible spin-orbit coupling effect. The band crossings were tracked experimentally and the complete nodal loop was identified quantitatively, which provide a critical experimental support for the existence of nodal-line fermions in the CaP_3 family of materials. Hosting simple topological nontrivial bulk electronic states around E_F and without complication from the trivial states, $SrAs_3$ is expected to be a potential platform for topological quantum state investigation and applications.

DOI: 10.1103/PhysRevLett.124.056402

Topological semimetals, as the nontrivial extension of topological classification of electronic quantum states from insulators to metals, are a group of materials in which the conduction and valence bands cross and form nodes behaving as monopole of a Berry flux [1,2]. When the nodes are close to the Fermi energy (E_F), the low-energy quasiparticle excitations would be drastically different from that of the conventional Schrödinger-type fermions and thus lead to novel transport properties, which are crucial to further studies of novel quantum states and modern quantum devices [3,4]. Some distinct point-contact nodes, e.g., fourfold, twofold, and threefold degenerate nodes, have been confirmed in Dirac [5,6], Weyl [7–14], and triply degenerate semimetals [15–25] in previous studies, respectively. While, line-contact nodes, i.e., nodal lines, with their various configurations [26] have not been fully investigated in experiments until now.

The nodal ring, nodal link and nodal chain all belong to nodal-line systems in which nodes extend along one-dimensional lines instead of discrete points in the three-dimensional (3D) Brillouin zone (BZ) [3,26–45]. Theories have predicted that a nontrivial Berry phase around the nodal line would generate a half-integer shift of Landau-level index [29] and result in drumheadlike surface states [28,30]. To date, nodal-line states have been theoretically proposed and then experimentally confirmed in several compounds, including CaAgX (X = P, As) [31,32], $PbTaSe_2$ [33], ZrSiS [34–38], and MB_2 (M = Ti, Zr) [39–43]. However, for most of these compounds, topological nontrivial band-crossing nodes are enclosed by complex trivial bulk or surface bands, which would complicate potential applications of these topological nodal-line semimetals.

Very recently, the CaP_3 family of materials have been predicted to possess topological nodal rings with two-dimensional drumheadlike surface states, which are protected by the spatial-inversion and time-reversal symmetries, with and without a certain mirror symmetry [44,45]. Specifically, for the monoclinic semimetal $SrAs_3$, a nodal loop was proposed to be located in the vicinity of E_F,

without the distraction of complicated topological trivial Fermi surfaces (FSs). If the spin-orbit coupling (SOC) is considered, a small gap would open along the loop, resulting in a strong topological insulator [45,46]. Actually, magnetoresistance (MR) and Shubnikov–de Haas quantum oscillation measurements on the single-crystal $SrAs_3$ have revealed the negative MR induced by the chiral anomaly and the nontrivial π Berry phase, which strongly suggest the existence of topological nodal-line semimetal states therein [47,48]. However, so far direct spectroscopic evidence of such novel band structure on that is still absent.

In this Letter, we provide compelling evidence for Dirac nodal-line fermions in the monoclinic semimetal $SrAs_3$ by means of angle-resolved photoemission spectroscopy (ARPES) and first-principles calculations. Our calculations suggest that a single nodal loop should be located on the Γ-Y-S plane, which will not be distracted by complicated topologically trivial FSs. Further detailed photon-energy-dependent ARPES measurements on the naturally cleaved (010) surfaces of $SrAs_3$ unambiguously reveal the complete nodal-line feature around the Y point, which well reproduces calculations along the corresponding paths in the BZ and demonstrates the existence of nodal-line fermions in the CaP_3 family definitely.

High-quality single crystals of $SrAs_3$ were grown by solid-phase sintering reaction using stoichiometric amounts of Sr and As as described elsewhere [47]. ARPES measurements were performed at 13U beam line of National Synchrotron Radiation Laboratory (NSRL), Dreamline and 03U beam lines of Shanghai Synchrotron Radiation Facility (SSRF), and One-Squared ARPES end station at BESSY II (see experimental details in the Supplemental Material [49]). The energy and angular resolutions were set to around 10 meV and 0.2°, respectively. All samples were cleaved under a vacuum greater than 5×10^{-11} Torr. During measurements, the temperature was kept at $T = 20$ K. The density functional theory (DFT) calculations were performed by using the linearized augmented plane wave method as implemented in WIEN2K [53] combined with Perdew-Burke-Ernzerhof form of the general gradient approximation (GGA) to the exchange-correlation functional [54]. Additionally, the modified Becke-Johnson (MBJ) potential [50–52] was employed for a reasonable correction, as GGA may give underestimated relative positioning of valance and conduction bands for semiconductors and semimetals. In order to explore the topological properties, a tight-binding model based on the maximally localized Wannier functions (MLWF) was constructed using the WANNIER90 [55,56] and WIEN2WANNIER [57] programs from DFT band structures. The surface spectral functions were calculated by the iterative Greens function method implemented in the WANNIERTOOLS code [58].

The crystal structure of $SrAs_3$ belongs to the simple monoclinic space group [$C2/m$ (No. 12)], in which Sr

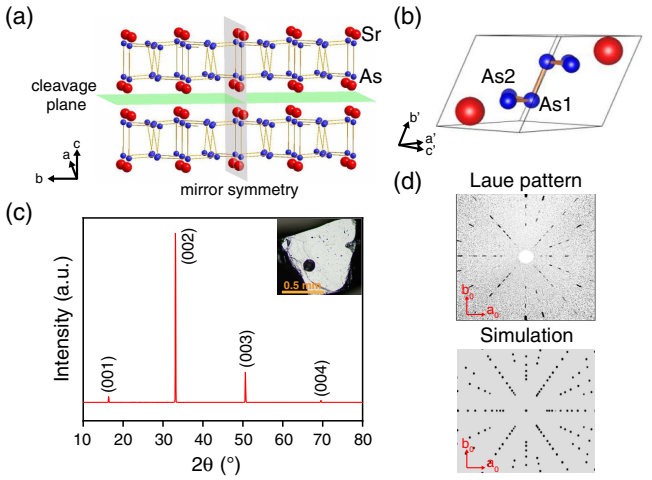

FIG. 1. (a) The side view of the crystal structure of $SrAs_3$. The atomic layers of As and Sr stack alternately along the c axis, and the natural cleavage and mirror symmetry planes are represented by the green and gray planes, respectively. (b) The monoclinic primitive cell of $SrAs_3$. (c) The single-crystal XRD measured on the (001) plane of the conventional lattice of $SrAs_3$. The inset shows the flat and shining cleavage plane. (d) The comparison between the x-ray Laue pattern taken on the cleaved sample (upper) and simulation (lower).

layers form channels in the a-b plane while As atoms are inserted into these channels, as illustrated in Fig. 1(a). It can be viewed as a list of infinite atomic layers of As and Sr stacking alternately along the c axis. Thus, the natural cleavage plane should be located at between the neighboring Sr layers [the green plane shown in Fig. 1(a)]. The lattice is reflection symmetric with respect to the -Sr-As-As-Sr- atomic plane marked by gray plane, and this crystallographic symmetry provides additional protection for the topological nontrivial electronic structure. Moreover, for this $C2/m$ space group compound, its primitive unit cell is shown in Fig. 1(b). It contains two types of As atoms, with As1 on the mirror plane and As2 on both sides.

Considering the sensitivity of electronic structure to the crystal structure and stoichiometry, we carefully characterized our $SrAs_3$ samples used for our experimental studies. We confirmed that these samples are pure phase with the molar ratio of Sr:As $= 1:3$ by using both the powder x-ray diffraction (XRD) and scanning electron microscope equipped with an energy dispersive x-ray spectrometer (EDS) (see Figs. S1 and S2 in the Supplemental Material [49]). After cleaved in the air, our samples show typical flat and shining surfaces [the inset of Fig. 1(c)], and these samples have been further characterized by the single-crystal XRD, as shown in Fig. 1(c). The results reveal their monoclinic crystal structure with the deduced lattice constants $a = 9.605(7)$ Å, $b = 7.665(3)$ Å, and $c = 5.873(1)$ Å, and $\alpha = \gamma = 90°$, $\beta = 112.869°$, in an excellent agreement with the previous report [59]. The single-crystal XRD measurement also indicates that the a-b plane should be

the natural cleavage plane stacking up along the c axis. Moreover, as shown in Fig. 1(d), the sharp x-ray Laue pattern taken from the cleaved sample can be well reproduced by the simulated result on the a-b plane, which further confirms the cleavage plane and high quality of our samples. We note that the naturally cleaved surface of $SrAs_3$ actually corresponds to the (010) plane of its primitive unit cell. In addition, the periodicity of $SrAs_3$ along the c direction of conventional unit cell is the same as this along the b direction of primitive unit cell. For simplicity, hereafter we will always use the primitive unit cell in our discussion.

Figure 2(a) illustrates the 3D BZ of the $SrAs_3$ primitive lattice, in which the gray plane (Γ-Y-S plane) stands for the mirror symmetry plane. According to the calculated band structure along high-symmetry lines [Fig. 2(c)], one can see that the band structure of $SrAs_3$ around E_F is rather simple. Except for a holelike band barely crossing E_F around Γ, there is a band crossing only around the Y point. Actually, our calculations further show that these two bands with opposite parities inversion in the vicinity of E_F only around Y in the whole BZ, as shown in Fig. 2(d). We also performed the orbital character analysis on the bands, and they are mainly derived from p orbitals of As atoms. The conduction band around the Y point is dominated by the As1-p_y orbital, while the valence band is mainly contributed by As2-p_x, As2-p_y, and As2-p_z orbitals [Fig. 2(d)]. Theoretically, with both the spatial-inversion and time-reversal symmetries conserved, the energy inverted bands with opposite parities have been proposed to cross along a closed nodal loop [45]. In the case of $SrAs_3$, calculations suggest that a closed Dirac nodal loop should surround the Y point on the Γ-Y-S plane, just as the red circle marked in Fig. 2(a). As illustrated in Fig. 2(f), our semi-infinite slab calculations clearly resolve the characteristic drumheadlike surface state around $\bar{Y}$ in the projected BZ along the k_c direction, which is nestled between two Dirac cones projected by the nodal loop in this direction. However, in the projected BZ along the $k_y(k_b)$ direction ($\bar{\Gamma}$-$\bar{X}$-$\bar{Z}$ plane), which is actually reachable by ARPES measurements on the cleaved surface of $SrAs_3$, the surface state is invisible since it is buried in the bulk states, as shown in Figs. 2(g) and 2(h). Besides, even when SOC is considered, the nodes would open a gap much smaller than those of other previously reported nodal-line semimetals, suggesting the weak SOC effect on its bulk electronic structure (see Fig. S4 in the Supplemental Material [49]). In these regards, ARPES measurements on (010) cleavage plane of $SrAs_3$ provide a unique opportunity for the investigation of the topological nodal line without the interference of other complicated bulk or surface states in the vicinity of E_F.

Since the predicted nodal loop in $SrAs_3$ is exactly perpendicular to the (010) cleavage plane, as shown in Figs. 2(a) and 2(b), a detailed photon-energy-dependent ARPES measurement on the k_x-k_y plane is highly desired to identify the whole nodal loop [Fig. 2(e)]. Figures 3(a) and 3(b) show photoemission intensity maps on the Γ-X-Y-M plane (k_x-k_y plane) taken at E_F and E_F-0.6 eV, respectively. Together with the corresponding calculated bulk constant energy surface on the k_x-k_y plane taken at E_F-0.6 eV, one can distinguish the warped chainlike band

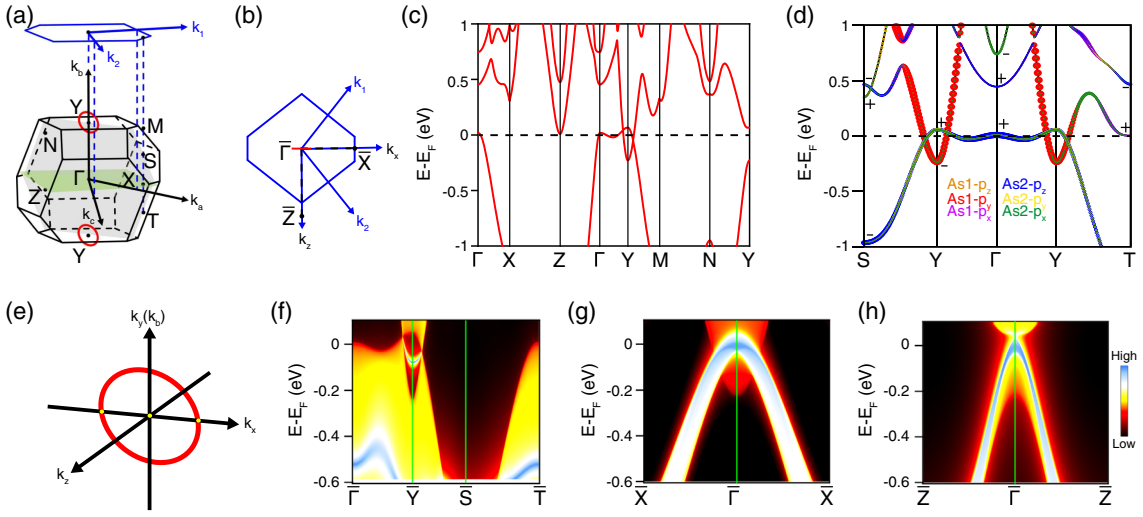

FIG. 2. (a) The 3D BZ of the $SrAs_3$ primitive lattice. The nodal loop (red ring) surrounds the Y point on the Γ-Y-S plane, i.e., the mirror symmetry plane. The green plane is perpendicular to the k_y (k_b) axis. (b) The projected BZ perpendicular to k_b. The red line is the projection of the nodal loop. k_1 and k_2 represent projections of k_a and k_c onto this plane, respectively. (c) The calculated band structure along high-symmetry paths without SOC. (d) The calculated band structure with orbital characters and parity analysis. (e) The schematic of the nodal loop on the k_x-k_y plane. (f) The calculated surface state in the projected BZ along the k_c direction ($\bar{\Gamma}$-$\bar{Y}$-$\bar{S}$ plane). The drumheadlike surface state is nestled between two solid Dirac cones, which are the projection of the nodal loop. (g),(h) Calculated band structure along different high-symmetry paths in the project BZ along the k_y direction ($\bar{\Gamma}$-$\bar{X}$-$\bar{Z}$ plane).

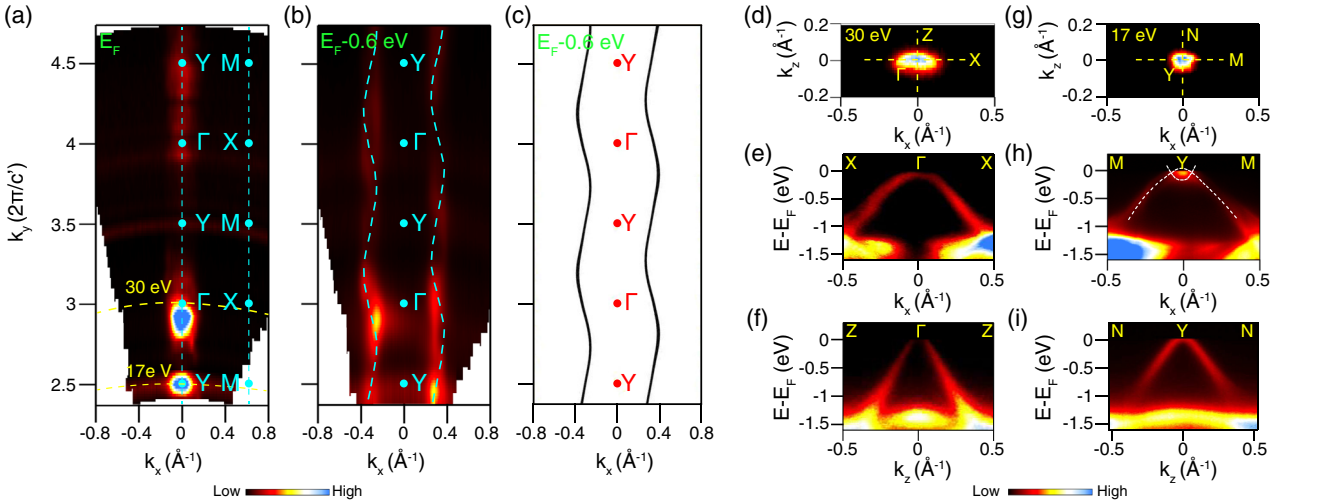

FIG. 3. (a),(b) Integrated photoemission intensity maps in the k_x-k_y plane taken at E_F and E_F-0.6 eV, respectively. The photon energies used for the k_y dispersion measurement were from 14 to 86 eV. The measurement with low photon energies (14–30 eV) was performed at 13U beam line of NSRL. The measurement with high photon energies (30–86 eV) was performed at Dreamline beam line of SSRF. (c) Corresponding calculated bulk constant energy surface on the k_x-k_y plane taken at E_F-0.6 eV. (d),(g) Integrated photoemission intensity maps in the Γ-X-Z ($hv = 30$ eV) plane and Y-M-N ($hv = 17$ eV) plane, respectively. (e),(f) Photoemission intensity plots taken along Γ-X and Γ-Z, respectively. (h),(i) Photoemission intensity plots taken along Y-M and Y-N, respectively.

feature with a pronounced periodic modulation along the k_y direction, as shown in Figs. 3(b) and 3(c). With an inner potential of 15.7 eV and $c' = 5.411$ Å (the vertical distance between the adjacently equivalent As-atom layers along c), we fitted the periodic variation according to the free electron final-state model [60]. We found that $hv = 30$, 60, and 99 eV are close to the Γ point, and 17, 43, 78, and 122 eV are close to the Y point [49]. However, due to matrix element effect, the nodal-line dispersions near E_F can only be clearly observed under low-energy photons (around 17 eV), which are mainly used to determine the complete nodal-line structure.

Figures 3(d)–3(i) show FSs and photoemission intensity plots taken with 30 and 17 eV photons, which correspond to band structure on the Γ-X-Z and Y-M-N high-symmetry planes, respectively. On the Γ-X-Z plane, the FS is an elliptical pocket [Fig. 3(d)], and band dispersions along the Γ-X and Γ-Z directions exhibit anisotropic structures, as the bands displayed in Figs. 3(e) and 3(f), respectively. On the Y-M-N plane, the FSs and band structure are rather similar to those on the Γ-X-Z plane, as shown in Figs. 3(g)–3(i). The main difference of band structure between these two high-symmetry planes lies in the existence of an additional inverted band structure producing nodes around the Y point, as highlighted by the white dashed lines in Fig. 3(h). Note that such band inversion can be only observed along the Y-M direction, but is totally absent along Y-N, which is in a good agreement with our calculations in Figs. 2(g) and 2(h). Actually, around Y, the cuts along the Y-M (k_x) and Y-N (k_z) directions both pass through the center of the nodal loop. However, the Y-M cut has two intersections with the loop, while the Y-N has no intersection with the loop, as illustrated in Fig. 2(e). Moreover, for the band crossings occurring along the Y-M line, we did not resolve any visible lifting of the node degeneracy, indicating the negligible SOC effect in this compound.

In order to determine the complete nodal-line feature, we carried out a high-resolution ARPES survey around Y in the k_x-k_y plane with varying photon energies, as illustrated in Fig. 4. When the photon energy is changed, the cut moves almost vertically up and down along the k_y direction. As shown in Fig. 4(a), when the ARPES cut passes exactly the Y point (taken at 17 eV), the electronlike band and holelike band cross and form two nodes, in a remarkable agreement with calculations (white lines). As the cuts move gradually away from the Y point, the band-crossing area shrinks gradually and finally disappears. Such an evolution of this elliptical nodal loop in $SrAs_3$ with the change of k_y has been clearly demonstrated. Here, both our experimental (blue solid dots) and theoretical results (the red line) can profile the complete nodal loop in $SrAs_3$. Figure 4(b) shows the corresponding energy-distribution curves (EDCs), which further demonstrate clearly the nodes formed by the band crossings and their evolution with k_y. Moreover, we determined quantitatively the size of the nodal loop from the experimental data, as marked by blue dots in Fig. 4(c). We found that the sizes of nodal loop along the k_y and k_x directions are 0.22 ± 0.03 Å^{-1} and 0.15 ± 0.03 Å^{-1}, respectively, which are in a good agreement with the prediction of calculations. Thus, we have unambiguously tracked the nodes and identified the topological nontrivial nodal line in this prototypical topological semimetal.

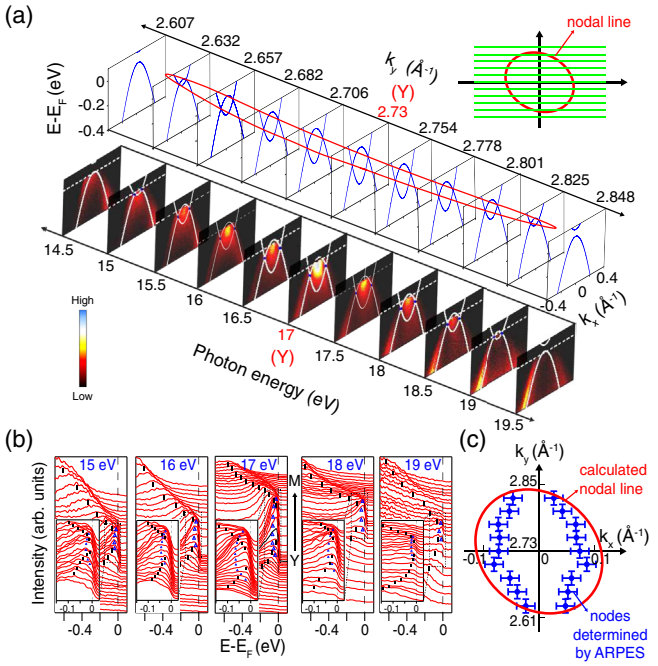

FIG. 4. (a) Band dispersions along the $\bar{Y}$-$\bar{M}$ direction taken with different photon energies, and the calculations are illustrated by white lines for comparison. These blue dots represent nodes. The inset shows the schematic of ARPES cuts crossing the nodal loop along k_y on the k_x-k_y plane. Green lines represent ARPES cuts at different k_y positions, which are taken with different photon energies. The red ring stands for the nodal loop. (b) Corresponding EDCs taken at different photon energies. (c) The comparison between nodal loops determined by ARPES (blue dots) and calculations (the red ring).

In summary, by using ARPES in combination with first-principles calculations, we unambiguously demonstrate the existence of Dirac nodal-line fermions in the monoclinic semimetal $SrAs_3$, which are under the protection of the spatial-inversion and time-reversal symmetries in the $C2/m$ symmetry material. With weak SOC effect and no interfering with complicated topological trivial states in the vicinity of E_F, $SrAs_3$ provides a good platform for further studies into Dirac nodal-line fermions.

We acknowledge Dr. L. L. Wang and Dr. H. Jin for their helpful discussion. This work was supported by the National Key R&D Program of the MOST of China (Grants No. 2016YFA0300204 and No. 2016YFA0302300), the National Science Foundation of China (Grants No. 11574337, No. 11704394, No. 11674030, and No. 11822405), and the Fundamental Research Funds for the Central Universities (Grant No. 310421113). Part of this research used Beam line 03U of the Shanghai Synchron Radiation Facility, which is supported by ME2 project under Contract No. 11227902 from National Natural Science Foundation of China. D. W. S. is supported by "Award for Outstanding Member in Youth Innovation Promotion Association CAS." The calculations used high performance computing clusters of Beijing Normal University in Zhuhai and the National Supercomputer Center in Guangzhou. We have been aware of a recent ARPES work on $SrAs_3$ with different results with ours [61]. Their samples were grown by the Sn-self flux technique, while ours were grown by the solid-phase sintering reaction method without any fluxes. We stress that our samples have been strictly characterized by detailed XRD and EDS to confirm their pure phase and right stoichiometry.

*Y. K. S. and G. W. W. contributed equally to this work.
†yinzhiping@bnu.edu.cn
‡lzh17@mail.sim.ac.cn
§dwshen@mail.sim.ac.cn

[1] G. E. Volovik, *The Universe in a Helium Droplet* (Oxford University Press on Demand, New York, 2003), Vol. 117.
[2] Z. Fang, N. Nagaosa, K. S. Takahashi, A. Asamitsu, R. Mathieu, T. Ogasawara, H. Yamada, M. Kawasaki, Y. Tokura, and K. Terakura, Science **302**, 92 (2003).
[3] A. A. Burkov, M. D. Hook, and L. Balents, Phys. Rev. B **84**, 235126 (2011).
[4] C.-K. Chiu, J. C. Y. Teo, A. P. Schnyder, and S. Ryu, Rev. Mod. Phys. **88**, 035005 (2016).
[5] Z. Liu, B. Zhou, Y. Zhang, Z. Wang, H. Weng, D. Prabhakaran, S.-K. Mo, Z. Shen, Z. Fang, X. Dai *et al.*, Science **343**, 864 (2014).
[6] S. Borisenko, Q. Gibson, D. Evtushinsky, V. Zabolotnyy, B. Büchner, and R. J. Cava, Phys. Rev. Lett. **113**, 027603 (2014).
[7] S.-Y. Xu, I. Belopolski, N. Alidoust, M. Neupane, G. Bian, C. Zhang, R. Sankar, G. Chang, Z. Yuan, C.-C. Lee *et al.*, Science **349**, 613 (2015).
[8] S.-M. Huang, S.-Y. Xu, I. Belopolski, C.-C. Lee, G. Chang, B. Wang, N. Alidoust, G. Bian, M. Neupane, C. Zhang *et al.*, Nat. Commun. **6**, 7373 (2015).
[9] X. Huang, L. Zhao, Y. Long, P. Wang, D. Chen, Z. Yang, H. Liang, M. Xue, H. Weng, Z. Fang *et al.*, Phys. Rev. X **5**, 031023 (2015).
[10] B. Q. Lv, H. M. Weng, B. B. Fu, X. P. Wang, H. Miao, J. Ma, P. Richard, X. C. Huang, L. X. Zhao, G. F. Chen, Z. Fang, X. Dai, T. Qian, and H. Ding, Phys. Rev. X **5**, 031013 (2015).
[11] H. Weng, C. Fang, Z. Fang, B. A. Bernevig, and X. Dai, Phys. Rev. X **5**, 011029 (2015).
[12] N. Xu, H. Weng, B. Lv, C. E. Matt, J. Park, F. Bisti, V. N. Strocov, D. Gawryluk, E. Pomjakushina, K. Conder *et al.*, Nat. Commun. **7**, 11006 (2016).
[13] S.-Y. Xu, N. Alidoust, I. Belopolski, Z. Yuan, G. Bian, T.-R. Chang, H. Zheng, V. N. Strocov, D. S. Sanchez, G. Chang *et al.*, Nat. Phys. **11**, 748 (2015).
[14] L. Yang, Z. Liu, Y. Sun, H. Peng, H. Yang, T. Zhang, B. Zhou, Y. Zhang, Y. Guo, M. Rahn *et al.*, Nat. Phys. **11**, 728 (2015).
[15] H. Weng, C. Fang, Z. Fang, and X. Dai, Phys. Rev. B **93**, 241202(R) (2016).
[16] Z. Zhu, G. W. Winkler, Q. S. Wu, J. Li, and A. A. Soluyanov, Phys. Rev. X **6**, 031003 (2016).

[17] G. Chang, S.-Y. Xu, S.-M. Huang, D. S. Sanchez, C.-H. Hsu, G. Bian, Z.-M. Yu, I. Belopolski, N. Alidoust, H. Zheng *et al.*, Sci. Rep. **7**, 1688 (2017).

[18] B. Lv, Z.-L. Feng, Q.-N. Xu, X. Gao, J.-Z. Ma, L.-Y. Kong, P. Richard, Y.-B. Huang, V. Strocov, C. Fang *et al.*, Nature (London) **546**, 627 (2017).

[19] B. Bradlyn, J. Cano, Z. Wang, M. Vergniory, C. Felser, R. J. Cava, and B. A. Bernevig, Science **353**, aaf5037 (2016).

[20] G. Chang, S.-Y. Xu, B. J. Wieder, D. S. Sanchez, S.-M. Huang, I. Belopolski, T.-R. Chang, S. Zhang, A. Bansil, H. Lin *et al.*, Phys. Rev. Lett. **119**, 206401 (2017).

[21] P. Tang, Q. Zhou, and S.-C. Zhang, Phys. Rev. Lett. **119**, 206402 (2017).

[22] G. Chang, B. J. Wieder, F. Schindler, D. S. Sanchez, I. Belopolski, S.-M. Huang, B. Singh, D. Wu, T.-R. Chang, T. Neupert *et al.*, Nat. Mater. **17**, 978 (2018).

[23] Z. Rao, H. Li, T. Zhang, S. Tian, C. Li, B. Fu, C. Tang, L. Wang, Z. Li, W. Fan *et al.*, Nature (London) **567**, 496 (2019).

[24] D. S. Sanchez, I. Belopolski, T. A. Cochran, X. Xu, J.-X. Yin, G. Chang, W. Xie, K. Manna, V. Süß, C.-Y. Huang *et al.*, Nature (London) **567**, 500 (2019).

[25] D. Takane, Z. Wang, S. Souma, K. Nakayama, T. Nakamura, H. Oinuma, Y. Nakata, H. Iwasawa, C. Cacho, T. Kim *et al.*, Phys. Rev. Lett. **122**, 076402 (2019).

[26] T. Bzdušek, Q. Wu, A. Rüegg, M. Sigrist, and A. A. Soluyanov, Nature (London) **538**, 75 (2016).

[27] C. Fang, Y. Chen, H.-Y. Kee, and L. Fu, Phys. Rev. B **92**, 081201(R) (2015).

[28] C. Fang, H. Weng, X. Dai, and Z. Fang, Chin. Phys. B **25**, 117106 (2016).

[29] Z. Yan, R. Bi, H. Shen, L. Lu, S.-C. Zhang, and Z. Wang, Phys. Rev. B **96**, 041103(R) (2017).

[30] R. Yu, Z. Fang, X. Dai, and H. Weng, Front. Phys. **12**, 127202 (2017).

[31] X.-B. Wang, X.-M. Ma, E. Emmanouilidou, B. Shen, C.-H. Hsu, C.-S. Zhou, Y. Zuo, R.-R. Song, S.-Y. Xu, G. Wang *et al.*, Phys. Rev. B **96**, 161112(R) (2017).

[32] A. Yamakage, Y. Yamakawa, Y. Tanaka, and Y. Okamoto, J. Phys. Soc. Jpn. **85**, 013708 (2016).

[33] G. Bian, T.-R. Chang, R. Sankar, S.-Y. Xu, H. Zheng, T. Neupert, C.-K. Chiu, S.-M. Huang, G. Chang, I. Belopolski *et al.*, Nat. Commun. **7**, 10556 (2016).

[34] M. M. Hosen, K. Dimitri, I. Belopolski, P. Maldonado, R. Sankar, N. Dhakal, G. Dhakal, T. Cole, P. M. Oppeneer, D. Kaczorowski *et al.*, Phys. Rev. B **95**, 161101(R) (2017).

[35] R. Lou, J.-Z. Ma, Q.-N. Xu, B.-B. Fu, L.-Y. Kong, Y.-G. Shi, P. Richard, H.-M. Weng, Z. Fang, S.-S. Sun *et al.*, Phys. Rev. B **93**, 241104(R) (2016).

[36] L. M. Schoop, M. N. Ali, C. Straßer, A. Topp, A. Varykhalov, D. Marchenko, V. Duppel, S. S. Parkin, B. V. Lotsch, and C. R. Ast, Nat. Commun. **7**, 11696 (2016).

[37] D. Takane, Z. Wang, S. Souma, K. Nakayama, C. Trang, T. Sato, T. Takahashi, and Y. Ando, Phys. Rev. B **94**, 121108(R) (2016).

[38] B.-B. Fu, C.-J. Yi, T.-T. Zhang, M. Caputo, J.-Z. Ma, X. Gao, B. Lv, L.-Y. Kong, Y.-B. Huang, P. Richard *et al.*, Sci. Adv. **5**, eaau6459 (2019).

[39] X. Feng, C. Yue, Z. Song, Q. S. Wu, and B. Wen, Phys. Rev. Mater. **2**, 014202 (2018).

[40] Z. Liu, R. Lou, P. Guo, Q. Wang, S. Sun, C. Li, S. Thirupathaiah, A. Fedorov, D. Shen, K. Liu *et al.*, Phys. Rev. X **8**, 031044 (2018).

[41] R. Lou, P. Guo, M. Li, Q. Wang, Z. Liu, S. Sun, C. Li, X. Wu, Z. Wang, Z. Sun *et al.*, npj Quantum Mater. **3**, 50 (2018).

[42] X. Zhang, Z.-M. Yu, X.-L. Sheng, H. Y. Yang, and S. A. Yang, Phys. Rev. B **95**, 235116 (2017).

[43] C.-J. Yi, B. Q. Lv, Q. S. Wu, B.-B. Fu, X. Gao, M. Yang, X.-L. Peng, M. Li, Y.-B. Huang, P. Richard, M. Shi, G. Li, O. V. Yazyev, Y. G. Shi, T. Qian, and H. Ding, Phys. Rev. B **97**, 201107(R) (2018).

[44] Y. Quan, Z. P. Yin, and W. E. Pickett, Phys. Rev. Lett. **118**, 176402 (2017).

[45] Q. Xu, R. Yu, Z. Fang, X. Dai, and H. Weng, Phys. Rev. B **95**, 045136 (2017).

[46] L. Fu, C. L. Kane, and E. J. Mele, Phys. Rev. Lett. **98**, 106803 (2007).

[47] S. Li, Z. Guo, D. Fu, X.-C. Pan, J. Wang, K. Ran, S. Bao, Z. Ma, Z. Cai, R. Wang *et al.*, Science bulletin **63**, 535 (2018).

[48] L. An, X. Zhu, W. Gao, M. Wu, W. Ning, and M. Tian, Phys. Rev. B **99**, 045143 (2019).

[49] See Supplemental Material at http://link.aps.org/supplemental/10.1103/PhysRevLett.124.056402 for details of single-crystals characterization, ARPES experiments, and theoretical calculations, which includes Refs. [45–47,50–52].

[50] F. Tran and P. Blaha, Phys. Rev. Lett. **102**, 226401 (2009).

[51] W. Feng, D. Xiao, J. Ding, and Y. Yao, Phys. Rev. Lett. **106**, 016402 (2011).

[52] H. Zhang and S.-C. Zhang, Phys. Status Solidi RRL **7**, 72 (2013).

[53] P. Blaha, K. Schwarz, G. K. Madsen, D. Kvasnicka, and J. Luitz, *WIEN2K, An Augmented Plane Wave+ Local Orbitals Program for Calculating Crystal Properties* (Karlheinz Schwarz, Technische Universität Wien, Austria, 2001).

[54] J. P. Perdew, K. Burke, and M. Ernzerhof, Phys. Rev. Lett. **77**, 3865 (1996).

[55] N. Marzari, A. A. Mostofi, J. R. Yates, I. Souza, and D. Vanderbilt, Rev. Mod. Phys. **84**, 1419 (2012).

[56] A. A. Mostofi, J. R. Yates, Y.-S. Lee, I. Souza, D. Vanderbilt, and N. Marzari, Comput. Phys. Commun. **178**, 685 (2008).

[57] J. Kuneš, R. Arita, P. Wissgott, A. Toschi, H. Ikeda, and K. Held, Comput. Phys. Commun. **181**, 1888 (2010).

[58] Q. Wu, S. Zhang, H.-F. Song, M. Troyer, and A. A. Soluyanov, Comput. Phys. Commun. **224**, 405 (2018).

[59] W. Bauhofer, M. Wittmann, and H. Schnering, J. Phys. Chem. Solids **42**, 687 (1981).

[60] D. Liebowitz and N. J. Shevchik, Phys. Rev. B **17**, 3825 (1978).

[61] M. M. Hosen, B. Wang, G. Dhakal, K. Dimitri, F. Kabir, C. Sims, S. Regmi, T. Durakiewicz, D. Kaczorowski, A. Bansil *et al.*, arXiv:1812.06365.